Peer-reviewed version available at *Materials* **2019**, *12*, 663; doi:10.3390/ma12040663

Article

Alternative Process Routes to Manufacture Porous Ceramics – Opportunities and Challenges

Uwe Scheithauer [1,*], Florian Kerber [1], Alexander Füssel [1], Stefan Holtzhausen [2], Wieland Beckert [1], Eric Schwarzer [1], Steven Weingarten [1] and Alexander Michaelis [1]

[1] Fraunhofer Institute for Ceramic Technologies and Systems, Dresden, Germany;
[2] Technical University Dresden, Chair of Engineering Design and CAD, Dresden, Germany;
* Correspondence: uwe.scheithauer@ikts.fraunhofer.de; Tel.: +49-351-2557-7671

Abstract: Porous ceramics can be realized by different methods and are used for manifold applications, like cross-flow-membranes or wall-flow-filters, porous burners, solar receivers, structural design elements or catalytic supports. Within this paper three different alternative process routes are presented, which can be used to manufacture porous ceramic components with different properties or even graded porosity. The first process route bases on additive manufacturing (AM) of macro porous ceramic components, the second on AM of a polymeric template, which is used to manufacture porous ceramic components via replica technique. Finally, the third process route bases on an AM technology, which allows the manufacturing of multi-material or multi-property ceramic components, like components with dense and porous volumes in one complex shaped component.

Keywords: porous; ceramics; additive manufacturing; multi-material; multi-property; CerAMfacturing; CerAM VPP; CerAM T3DP; CerAM Replica

1. Introduction

Porous ceramics can be separated into those with mainly closed and others with mainly open porosity. In case of closed porosity, the single pores are not or only partially connected to each other and not accessible from the outer surface. This kind of porous material can be advantageous for lightweight components or applications where a high thermal shock resistance is necessary. In contrast, ceramics with a high amount of open porosity can be classified as a network of syndetic pores or cells. They are interesting for applications where a defined permeability for various fluids is required. For both types, open and closed pores, their size, size distribution, volume and shape determine the properties of the porous ceramics.

The preparation of porous ceramics can be realized by different methods. One way is the sintering of ceramic powders without significant densification. The resulting free space between the ceramic particles leads to a porosity from a few nanometers up to some micrometers (sometimes even millimeters), depending on the particle size distribution. With this method pore volumes up to 40% are achievable; interesting for example for cross-flow-membranes or wall-flow-filters [1].

Structures with higher amounts of porosity are often called foams, which can be prepared by the burn-out of pore formers, the direct foaming or the replication of a sacrificial template [2]. Up to 50% pore volume are attainable by the use of placeholders like organic or polymeric particles that evaporate or burn during the sintering step of the ceramic material. With this technique, pores of some micrometers up to some millimeters are formed [3]. Direct foaming by physical or chemical foaming mechanisms leads to pore volumes up to 70%. Due to destabilizing mechanisms such as coalescence and drainage, the pore size of those foams is often inhomogeneous distributed in one component, which includes a non-negligible amount of closed pores [4].

An open pore volume of up to 90% is achievable by the replica technique (Schwartzwalder method) [5]. Due to its high process stability, the possibility of automating and the therewith-reached

large production capacity, it is the most common process to fabricate open-celled foams. The result of the replication technique is an extremely open network of interconnected, but hollow struts. Depending on the chosen template, the structure can be regular or irregular.

Open-celled ceramic foams prepared by replication start from reticulated, netlike polymer foams, which are commercially available in various cell sizes. Classified by pores-per-inch (ppi) according to the ASTM-standard D3576-77, a wide range of polymeric foams is applicable: coarse ones with about 5 ppi have a medium pore size of around 5 mm while the pores of fine foams with down to 90 ppi reach only about 200 μm.

The unique structure of open-celled foams corresponds to outstanding properties like high specific surface area, low pressure drop, low density and high thermal shock stability. On that account, ceramic foams can not only be used for metal melt filtration, which is state of the art in the casting industry since decades [6], but also for a large number of highly sophisticated applications. Nowadays, these are manly porous burners [7], solar receivers [8], structural design elements or catalytic supports [9]. In all those applications, an adjusted flow behavior as well as a high mechanical and abrasion stability is mandatory. In addition, a high thermal and chemical resistance can be essential to reach increasing application temperatures in aggressive chemical environments.

Based on a statistically grown pore structure, ceramic foams are limited reading the cell sizes, strut thickness and surface area by the polymeric foam templates. Alternatively, technical textiles and especially additive manufactured templates enlarge the range of possible applications. Latter is one topic of this manuscript and will be described in detail below.

Within this paper different alternative process routes are presented, which can be used to manufacture porous ceramic components with different properties. The first process route bases on additive manufacturing (AM) of porous ceramic components and the main challenge is the generation of the necessary CAD data. Two different strategies are presented to create CAD data for ceramic components with very complex geometries. The second process route bases on AM of a polymeric template, which is used to manufacture porous ceramic components via replica technique. And the third process route bases on an AM technology, which allows the manufacturing of multi-material or multi-property ceramic components, like components with dense and porous volumes in one complex shaped component.

To highlight the AM of ceramic components towards the common and well-known AM techniques for polymers, we add the acronym “CerAM” to the names of the different techniques. “CerAM” stands for “CerAMfacturing” which summarizes all AM techniques which are used for the additive manufacturing of ceramic components at Fraunhofer IKTS Dresden [10].

2. Alternative process routes

2.1. CerAMfacturing of single-material porous ceramics

For the first process route we use the CerAM VPP technology (vat photo-polymerization) and a commercially available AM device (CeraFab 7500) of Lithoz, Vienna. A highly-particle filled photo-curable suspension is placed on the entire surface of a tub before the curing is initiated by selectively exposure with light to manufacture the current layer and to connect this with the layer which was manufactured before [11]. Only the green body is manufactured additively, for that reason it has to be debinded and sintered to realize the final ceramic component. Suspensions are commercially available for different ceramics, like alumina or zirconia, which allow the manufacturing of nearly dense ceramic components. The final components could have very complex geometries [12,13] and convince by very smooth surfaces and highly accurate features.

One strength of additive manufacturing is that it opens the door to completely new structures, which are not restricted by the principles of traditional design. But the workflow of most current CAD tools is focused on such traditional rules and concepts and so the setup of geometry models of some innovative structures for additive manufacturing is sometimes rather limited and laborious. A promising approach for efficiently creating structures - in particular periodic and/ or graded ones - with versatile shapes and features may be based on processing of parametric surfaces from

Preprints (www.preprints.org) | NOT PEER-REVIEWED | Posted: 4 February 2019 doi:10.20944/preprints201902.0027.v1

Peer-reviewed version available at Materials 2019, 12, 663; doi:10.3390/ma12040663

mathematical field functions. Isosurfaces may be used to simply create manifold structure surfaces and to separate domains. A huge variety of suited mathematical functions does exist (gyroids, lidinoids, harmonic surfaces ...), the variety of possible structural shapes may be further expanded by function combination and composition. Deliberate choice and variation of functional parameters allows to adjust and modify the structures to desired specification targets (volume content, cell size, wall thickness, ...) and even the creation of graded structures often turns out as a simple operation by spatial variation of parameters. The same principles (isosurfaces) in structure creation may be applied also to fields functions, that result from a numeric analysis of mathematical-physical models, representing a link to automated and straight forward structural design from model based component optimization techniques (topology optimization). Traditional, NURB kernel based, CAD tools have only limited capabilities to directly generate such structures and the process of geometry import from external software tools over stereolithographic formats (*.stl) may be very labor-intensive.

An alternative CAD approach that is perfectly compatible to the mathematical creation and to additive manufacturing process may be based on a voxel description of such structures. For instance, it dramatically simplifies the combining and merging process of different structures, features (holes, stabilizer rods) and elements (hulls, screens) by Boolean operations and is naturally compatible with multi-material object definition. A simple, straightforward export interface to 3d printing devices is possible via xy-image stacks, instead of error-prone *.stl topology files. A few open source and commercial voxel based geometry generators are available (VoxelBuilder, MKagicaVoxel, GeoDict, Monolith, et al.), mainly oriented on game development and often sparsely prepared on mathematical based structure generation. Alternatively advanced, state of the art mathematics software platforms (Mathematica, Matlab) include all the necessary tools (mathematical function/ large matrix/ logical operation + visualization + parallelization) to do that job. An example for this approach is presented in chapter 3.1.1.

In addition, voxel models can describe a surface in a higher discretization accuracy by the extension to *Distance Fields*. Instead of providing a voxel with the information whether it lies inside or outside an object, the Euclidean distance to the surface is stored. Furthermore, it is determined whether the voxel coordinate is inside the object or not. If it lies inside, the distance is taken as a negative value. A so-called *Signed Distance Field* is created (9) (10).

The Boolean operations described above are determined by voxelwise comparing two voxel datasets. It applies to the union of two objects: $dist(A \cup B) = \max(dist(A), dist(B))$, for the difference: $dist(A - B) = \min(dist(A), -dist(B))$ and for the intersection: $dist(A \cap B) = \min(dist(A), dist(B))$. Another advantage of these distance fields is the calculation of offsets. Only the scalar voxel intensities are calculated by the given distance. A conversion to isosurface models (e.g. triangle meshes) is possible without problems with known methods like the Marching Cubes algorithm [16]. The advantage over the binary variant lies in the more detailed representation of an object within a voxel data structure. Figure 1 illustrates this advantage.

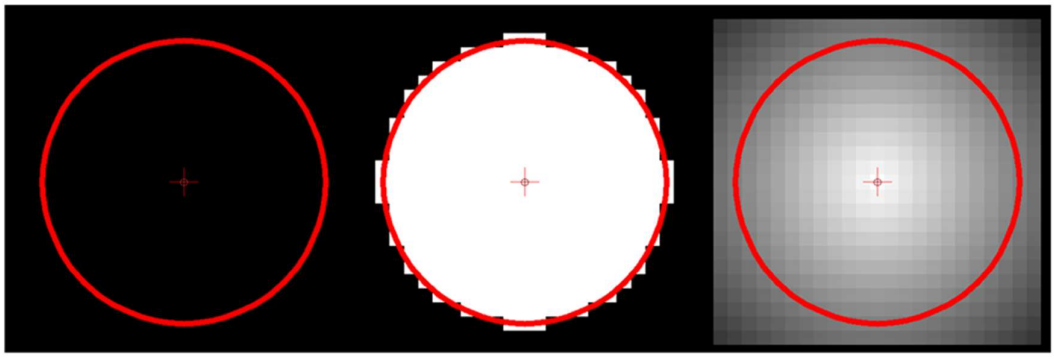

Figure 1: The approximation of a given circular contour (Left) in a binary voxel model (Center) allows only an inaccurate description. The use of signed distance fields (Right) and the interpolation-based recalculation of the contour is much more accurate.

Peer-reviewed version available at Materials 2019, 12, 663; doi:10.3390/ma12040663

2.2. CerAM Replica of single-material porous ceramics

One advantage of the replica technique is the opportunity to combine a well-established technology with the use of innovative, 3D structured components as templates. Designed for special purposes, the structural properties of that kind of replicated porous ceramics, such as pressure drop and geometrical surface area, correspond directly to the previously well-defined parameters.

Another important aspect, after sintering the ceramic, is the hollow space left by the decomposed polymeric template. While the hollow struts of ceramic foams are typically not useable but crucial with respect to the mechanical stability (sharp edges of the triangular polymeric foam strut), the cavities of porous ceramics based on additively manufactured, polymeric templates can be purposefully functionalized. Like buried channels in the walls of the structure, the cavities might be used for internal cooling or as an intensification of the heat exchange in a reactor (heating/cooling). Additionally, by using additive manufactured templates, it is possible to feed a reactor via perforations in the wall and their connection to the template cavities, which act as internal pipeline.

CerAM Replica represents the combination of the replica technique with 3D structured polymeric templates that have been manufactured additively. In this process, the polymeric 3D structures are coated with a ceramic suspension similar to reticulated foams or technical textiles. The suspension includes ceramic particles, organic and inorganic auxiliaries, such as dispersing agents, temporary binder, rheological additives and sintering aids. For an environment-friendly preparation and to avoid expensive equipment for explosion prevention, the suspensions are commonly water-based. The impregnation of the template is comparable to a dip coating. Excess suspension blocking the aspired open space in the structure can be removed by using rollers for flexible templates, or a centrifuge for rigid ones. This homogenization step is also useful to adjust a well-defined coating layer on the polymeric template. By using different coating suspensions and partially covering segments of the structure, connections between the later template-related cavities and the usable space can be achieved. Subsequently, the coated templates are dried, followed by the thermal treatment including the decomposition of the polymeric template and the sintering of the ceramic material.

2.3. CerAMfacturing of multi-property porous ceramics

Different challenges exist concerning the AM of multi-material or multi-property ceramics. Two or more different materials or suspension compositions have to be processed simultaneously in one AM process. Direct working AM technologies [17] are more suited than indirect working AM technologies because of the selective deposition of the material instead of the selective curing of a material, which was deposited on the entire building area. Latter requires a removing process for the first material to make room for the deposition of the second material or feedstock.

CerAM T3DP (Thermoplastic 3D Printing) is an AM technology, which bases on the selective deposition of molten, highly particle filled thermoplastic suspensions as single droplets [18,19]. These droplets are fused to generate 3D structures before the suspensions solidify because of the increasing viscosity resulting from cooling and the absence of shear forces. The portfolio of processible materials is nearly unlimited, which could be demonstrated for alumina, zirconia [18] and cemented carbide [20]. Furthermore, the suitability for AM of ceramic-based multi-material and multi-property components could be demonstrated, e.g. for combinations of stainless steel and zirconia [21,22], white and black zirconia [23] as well as the combination of dense and porous zirconia in one AM component [24].

The last combination is very interesting for applications like implants or catalytic support structures. But for the latter application alumina will be more interesting than zirconia because of the higher thermal conductivity and the lower material costs. The AM of alumina components by CerAM T3DP, which combine dense and porous volumes inside, is one topic of this paper and will be demonstrated below.

Preprints (www.preprints.org) | NOT PEER-REVIEWED | Posted: 4 February 2019 doi:10.20944/preprints201902.0027.v1

Peer-reviewed version available at Materials 2019, 12, 663; doi:10.3390/ma12040663

3. Materials and Methods

3.1. CerAMfacturing of porous ceramics by CerAM VPP

3.1.1. Generation of CAD-data by Voxel based geometry generators

A voxel based approach was applied to design and manufacture a demonstrator prototype for a novel three domain chemical reactor structure with integrated heat exchanger/ cooler structure, made up by a space-filling interwoven 3D network of three- among each other separated- domains.

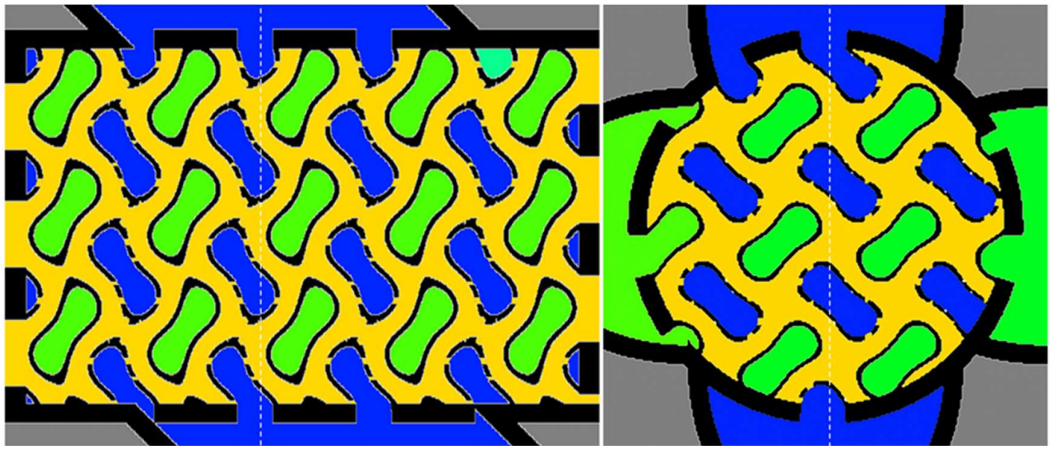

Figure 2: 2D sections of the reactor component to visualize the interconnected domain structure of fluid domains A (green), B (blue), C (yellow). White dashed lines label the position of the sections.

Two domains (fluid B and C), separated by perforated walls, may contain reactants while the third domain (fluid A) - enclosed by impermeable walls, may contain a heat carrier (or coolant) fluid. An integrated housing and media supply structure was formed, too, separating the main flow directions of the three fluids along the x, y, z direction by shadowing out the other domain areas at the housing inlet areas with shielding walls.

Mathematical basis of the interwoven three domain structure is the gyroid function:

$$K = \cos\left(\frac{2\pi}{\Delta L_x}\cdot(x-x_0)\right)\cdot\sin\left(\frac{2\pi}{\Delta L_y}\cdot(y-y_0)\right)+\cos\left(\frac{2\pi}{\Delta L_y}\cdot(y-y_0)\right)\cdot\sin\left(\frac{2\pi}{\Delta L_z}\cdot(z-z_0)\right)+\cos\left(\frac{2\pi}{\Delta L_z}\cdot(z-z_0)\right)\cdot\sin\left(\frac{2\pi}{\Delta L_x}\cdot(x-x_0)\right)$$

where choice of the isosurface-parameter K controls the position of the domain-wall surfaces; while ΔL_x, ΔL_y, ΔL_z define the period length of the structure along the x, y, z directions (may be functions of space to generate graded structures) and parameters x_0, y_0, z_0 allow a shifting of the structure in space. For the current example the fluid domains were specified by:

- fluid A: $K \leq -0.95$;
- fluid B: $0.95 \leq K$;
- fluid C: $-0.65 \leq K \leq 0.65$ and
- period length of the gyroid selected as $\Delta L_x = \Delta L_y = \Delta L_z = 6\,mm$.

The 3D gyroid core structure is shown in Figure 3. The voxel length was defined to initially 80 µm in x- and y-direction and 50 µm in z-direction, but was cut in half to 40 µm and 25 µm (corresponding to the physical resolution of the CerAM VPP device) in a final step by resizing the voxelized component structure by a array resample with scale factor 2 via linear interpolation in order to reduce the computing time and storage challenges from large 3D array operations. The total dimension of the full component (including integrated inlet- and outlet connects) was 1920x1080x1200 voxel.

The geometry definition was implemented in Mathematica 11, taking advantage of the comprehensive toolset of integrated functions and procedures for array and logical operations, optimised for the use of large arrays by condensed storage and parallelization. The developed workflow may be easily applied as a template for the generation of other structures and components.

Additionally to the generation of the gyroid structure a set of various parametrized cylinder and cuboid domains were created as basis domains for the cylindrical housing wall and pipe supply structures, shown in Figure 4. The full component geometry was shaped by Boolean combination of the various basic domains in voxelized form. The perforation in the wall between fluid A and B was created by applying a pattern of cylindrical holes to that wall structure, masking regions where the angle between drill and wall would become too steep. All domain and combining operations could be easily formulated by means of mathematical functions and operators.

For the generation of the structure a 256 GByte, 32 thread Windows workstation was applied, the total computation time for the full structure was about 10 h. The 3D voxel array was exported as an image stack of 1200 (*.png) 1920x1080 individual images to the software belonging to the CeraFab 7500 device.

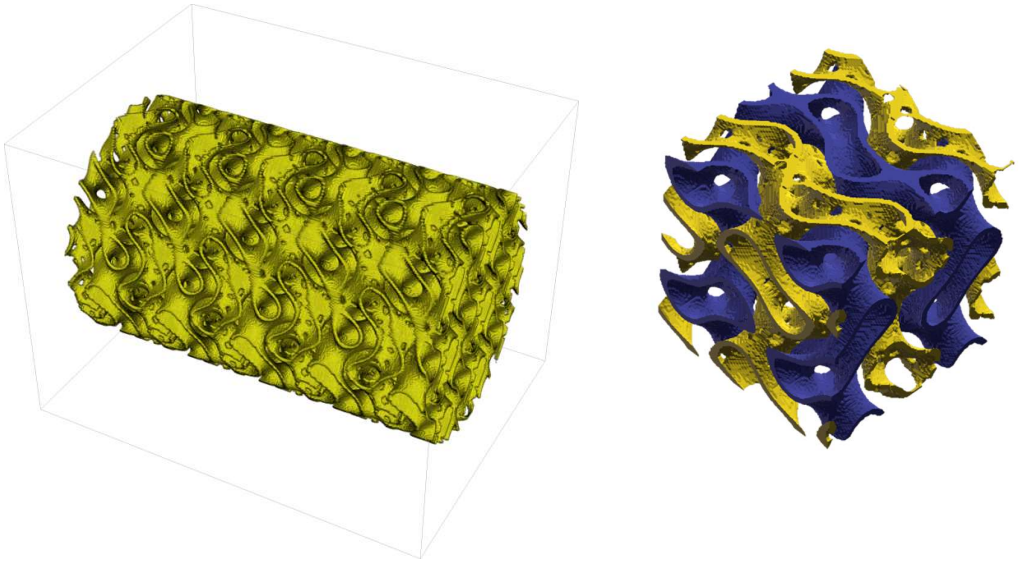

Figure 3: 3D gyroid core structure (left: full domain; right: detail; blue walls separating fluid A and C and yellow walls, separating fluid B and C) of the reactor component

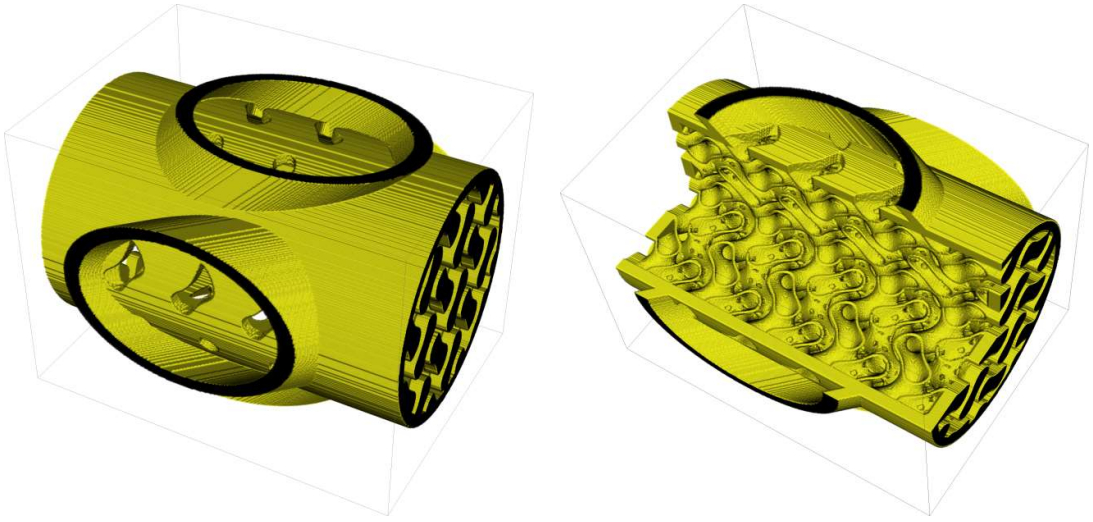

Figure 4: Housing of the gyroid structure (left) and sliced complete component (right)

Peer-reviewed version available at *Materials* **2019**, *12*, 663; doi:10.3390/ma12040663

3.1.2. Generation of CAD-data based on Distance Fields

The generation of porous structures based on *Distance Fields* is done by specifying a grid topology. This means a network of beam and node elements. A local dimension can be added to these. This allows the realization gradations within the porous structures (see Figure 5). Simple lattice topologies can be regular beam structures. But also complex, irregular topologies are possible. Figure 6 shows as an example, foam-like structures, which were created with a topology based on voronoi diagrams. The design space of a grid or porous structure is described by a *Signed Distance Field* of the object. This serves on the one hand to create the structure and on the other hand to mask later solid areas within the object. A signed distance field is also calculated for each topology element. Basic elements such as cylinders, cones and spheres can be used, but complex geometries are also possible, e.g. for adapting individual cross-section geometries. Boolean operations follow (see section *2.1*). A distinction is made between whether the generation is subtractive or additive. With the subtractive method, the geometry of the topology is subtracted from the design space model: $dist(R) = dist(A \cup !B)$. The additive method the geometry of the topology is generated directly: $dist(R) = dist(A \cup B)$. The subtractive method allows a setup of defined pore sizes, which can be necessary for medical applications (Figure 7).

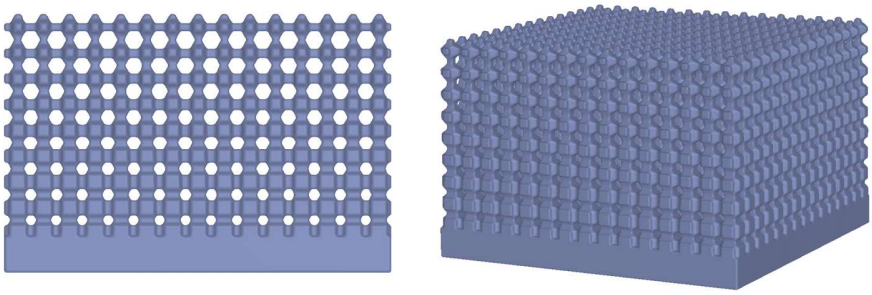

Figure 5: Graded porous structure of a cuboid. The pore size increases with increasing component height.

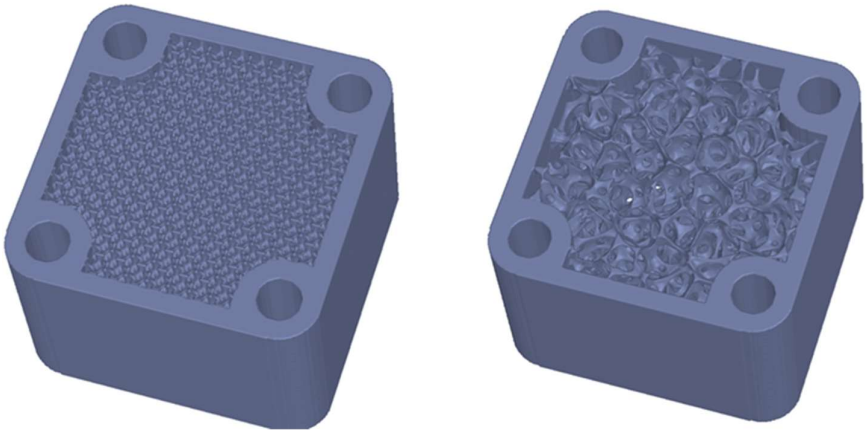

Figure 6: Example of an application with porous structures. A regular structure within the component geometry is shown on the left. On the right is a foam-like structure based on voronoi diagrams.

Peer-reviewed version available at Materials 2019, 12, 663; doi:10.3390/ma12040663

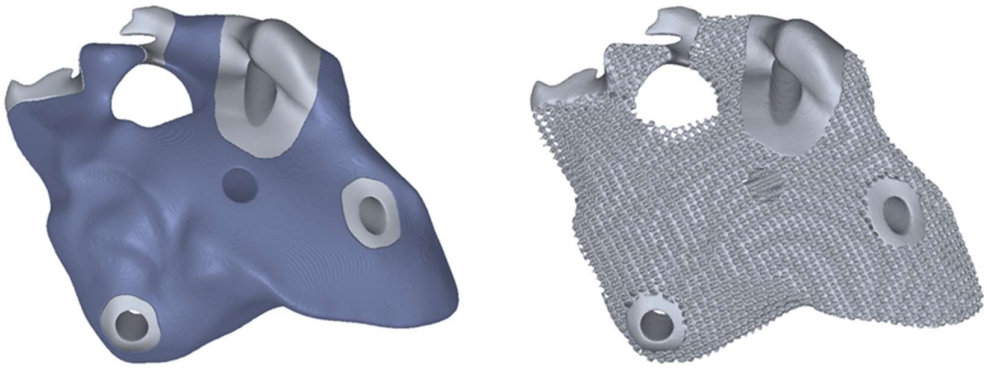

Figure 7: Another example shows the use of porous structures within an implant geometry. On the left you can see the definition of the Design Space for the lattice structure (dark blue), on the right the final implant design.

3.1.3. CerAM VPP

The CerAM VPP process is an AM process for ceramic components, used at the Fraunhofer IKTS, which is based on the digital light processing (DLP) technology. This technology was commercialized by Lithoz GmbH (Vienna, Austria), which sells suspensions and AM devices under the trade name lithography-based ceramic manufacturing (LCM). The AM device CeraFab7500 of Lithoz was the first commercially available printer for AM of dense ceramic components with a lateral resolution of 40 µm (pixel-size; 635 dpi) in xy-direction and 5-100 µm (layer thickness) in z-direction [11]. Complementary to DLP, a photoreactive suspension is deposited as complete layer exposed selectively by photons with a wavelength of 465 nm and a maximum intensity of 32.7 mW/cm². In various articles detailed descriptions of the process have been published [11-13,25,26]. The main advantages of this technology compared to other AM technologies for ceramic components are the high resolution, the high density of the sintered components as well as the surface quality of the final components.

Within this study a commercial available alumina suspension (Lithalox 350D; Lithoz) was used to build the specified ceramic demonstration components by CerAM VPP. The cleaning of the green bodies as well as the debinding and sintering (1650 °C, 2h) were done following the instructions given by Lithoz.

3.2. CerAM Replica of single-material porous ceramics

As demonstration example for CerAM Replica, a complex axially symmetric structure made of pressure-less sintered Silicon carbide has been prepared using a polymeric template generated by stereo lithography. In this demonstrator component crosslinked and tapered struts are circumferential arranged around a perforated cylinder. The structure was designed with the aid of SOLIDWORKS and transferred to a real component by using the CeraFab 7500 system from Lithoz. As material for AM of the template a mixture of different monomers, oligomers and photo-initiators, which is normally used as binder system for CerAM VPP suspensions, was chosen.

The ceramic coating suspension consisted of a SiC powder with a bi-modal particle size distribution and a highly carbon containing temporary binder. As sintering aid Boron and Carbon were used, added in the typical quantity of 0.5 and 2.5%. After the impregnation the samples were centrifuged for 10 seconds at 200 rpm. After the drying at 80 °C the samples were pyrolized at 1200 °C in order to decompose the template. The heat treatment was finalized with a sintering step at more than 2000 °C. The final reactor component of pressure-less sintered Silicon Carbide (SSiC) was intensively characterized by CT-analysis.

Preprints (www.preprints.org) | NOT PEER-REVIEWED | Posted: 4 February 2019 doi:10.20944/preprints201902.0027.v1

Peer-reviewed version available at Materials 2019, 12, 663; doi:10.3390/ma12040663

3.3. CerAMfacturing of multi-properties porous ceramics by CerAM T3DP

3.3.1. Generation of CAD-data and machine file

Figure 8 shows in the left the CAD-model of a honeycomb, which consist of two different parts. Each part will be printed with a different suspension to achieve dense (red) and porous (green) areas. The CAD-data were designed with the software tool SolidWorks. To generate the machine data the model was transformed into a g-code using the software Slic3r as shown in Figure 8 (right).

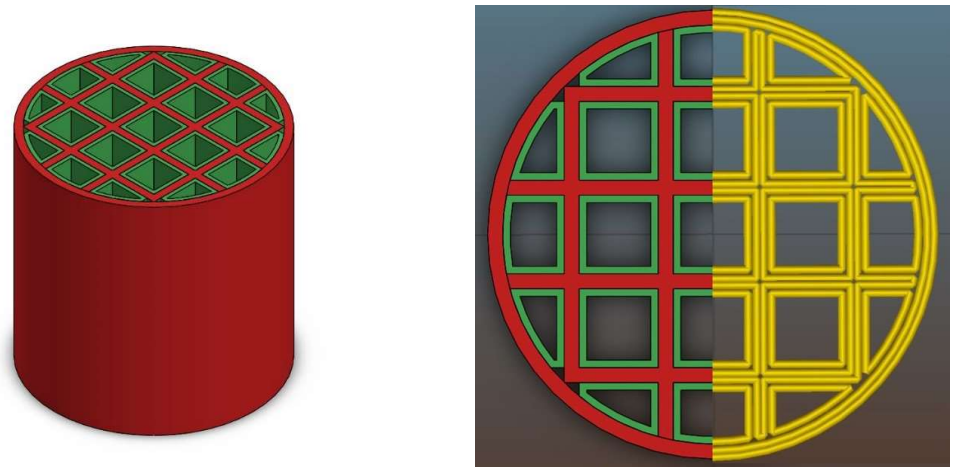

Figure 8: CAD-model of a honeycomb for two different materials (left) and visualization of the machine data (right)

3.3.2. CerAM T3DP

To prepare multi-functional components, like dense-porous components, particle-filled thermoplastic suspensions are needed, which result in dense and porous volumes after debinding and sintering. However, the ability for dispensing of the suspension have to be guaranteed. Three alumina powders with different characteristics were used.

Table shows the used powders with their specifications.

Table 1: characteristics of the used alumina powders.

name	company	d_{50} in µm	d_{90} in µm	fired density in g/cm³
CT 1200 SG	Almatis	1,734	3,14	3,99
Baikalox SMA6	Baikowski	0,251	0,671	3,96
MR52	Martinswerk	1,836	4,856	-

For each powder thermoplastic suspensions with different contents of pore forming agents (PFA) were prepared. As a PFA starch was used. The compositions of the prepared suspensions are presented in **Table**. The binder system, which consists of a mixture of different waxes, was molten at 100°C and stirred afterwards for about 15 minutes. Then a dispersant and the PFA was added and stirred for further 15 minutes. Afterwards the powder was added and homogenized for 2 hours.

Table 2: Compositions of the prepared suspensions.

component	content in vol.-%								
	A	B	C	D	E	F	G	H	I
CT1200 SG	50	50	45						
SMA6				35	35	45	55		

Preprints (www.preprints.org) | NOT PEER-REVIEWED | Posted: 4 February 2019 doi:10.20944/preprints201902.0027.v1

Peer-reviewed version available at Materials 2019, 12, 663; doi:10.3390/ma12040663

MR52									50	50
binder system	45	35	40	60	50	50	40	45	35
dispersant	5	5	5	5	5	5	5	5	5
PFA	0	10	10	0	10	0	0	0	10

To investigate the density, which is achievable with the different suspensions, small samples (16mm x 16mm x 10mm) were printed with each suspension and sintered at 1250 °C or 1600 °C. The density was measured in accordance with DIN EN 623-2.

Different pairs of thermoplastic suspensions were used to manufacture the multi-material components additively by CerAM T3DP. The red marked areas in **Error! Reference source not found.Figure** were printed with a suspension without any additives, which results in dense microstructure in the sintered component. This is necessary to achieve a sufficient strength and gas impermeability. To realize porous structures with a high specific surface area (green marked in **Error! Reference source not found.**) suspensions with PFA were used. Tests with suspensions with a PFA-content of more than 10 vol.-% were not successfully, because it was not possible to deposit the suspension reproducibly.

4. Results

4.1. CerAM VPP

4.1.1. CerAM VPP – machine files

The final designs were sliced by special slicing tools to generate the exposure maps for each layer (1-bit black-and-white image), which could be transferred directly to the software of the CeraFab 7500.

4.1.2. CerAM VPP – sintered components

Figure 9 shows the sintered alumina components additively manufactured by CerAM VPP. On the left side the sliced version of the reactor component is shown. It was sliced within the CAD-data and manufactured as ¾-component to make the inner structure visible. All channels and even the small holes between the different systems are open. On the right side of Figure 9 an alumina component according to Figure 6 (right) with graded porosity and pore size distribution is shown.

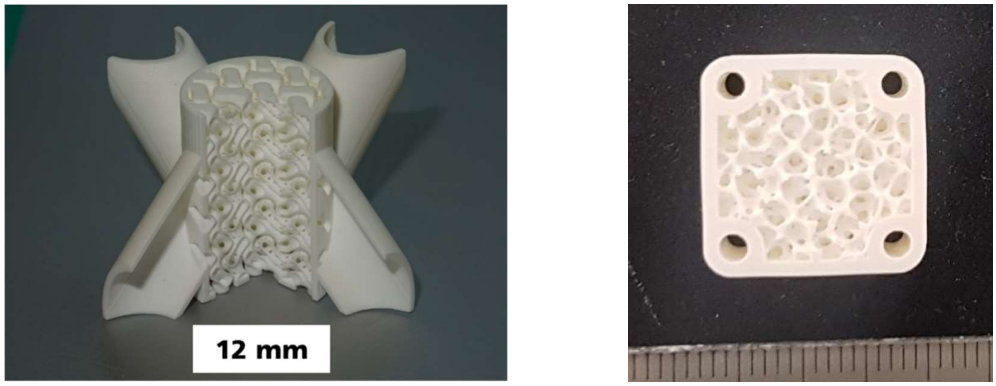

Figure 9: Sintered alumina components additively manufactured by CerAM VPP. On the left side a sliced version of the reactor component and on the right side a ceramic component with graded porosity and pore size distribution inside.

4.1.3. CerAM VPP – characterization

One of the most challenging steps within the process chain for CerAM VPP is the cleaning step. Any non-cured suspension has to be removed to avoid the clocking of the inner channels. CT scans

Peer-reviewed version available at Materials 2019, 12, 663; doi:10.3390/ma12040663

were done to assess the inner structure of the sintered components. Figure 10 shows two images of cross sections for the complete reactor component, oriented in xy- and xz-direction. It becomes visible that all channels and holes are open, only at the bottom there are residues of non-cured suspension, but in this section of the component it is not critical. The accumulation of non-cured suspension is a typical phenomenon for CerAM VPP, because during the thermal treatment the viscosity and wetting behavior is decreased. Due to this, the non-cured suspension accumulates at the bottom of the component cause by gravity, before it is cured thermally, debinded and sintered.

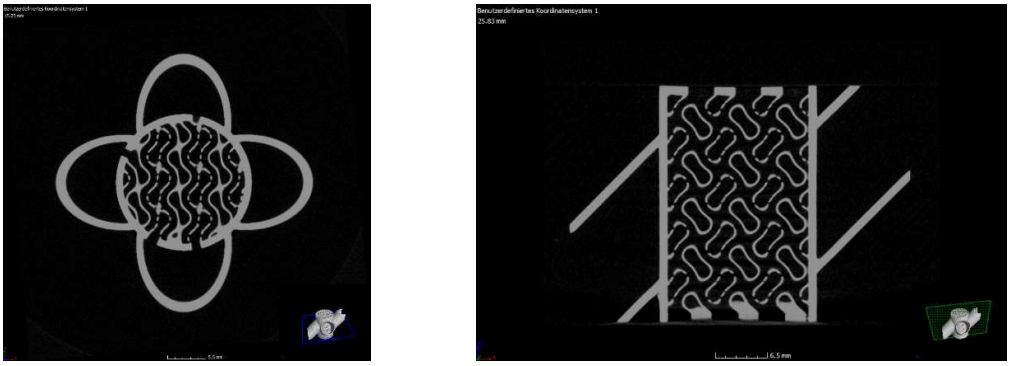

Figure 10: Cross-section images recalculated from the CT scan of the sintered alumina reactor component.

Figure 11 shows different images of the alumina component with graded porosity (Figure 9, right). On the left side the fine pore structure at the bottom of the component is shown, on the right side the structure with bigger pores on the top. In between there is a cross section in xz-direction generates from the CT data, which makes the vertically graded porosity visible.

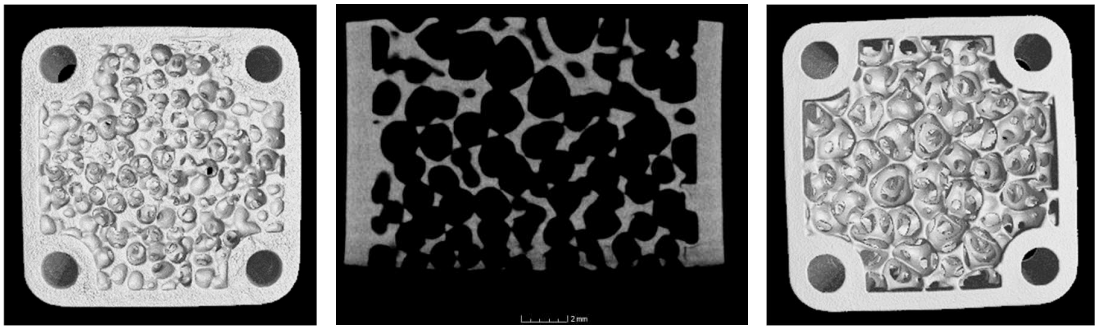

Figure 11: CT scan images of the sintered alumina component with graded porosity. Left: bottom; Right: top; cross-section image recalculated from the CT scan (middle)

4.2. CerAM Replica

4.2.1. CerAM Replica – final CAD-Data and polymeric template

The prepared CAD model of the structure was converted into a compatible format for the stereolithographic generation (*.stl). A perforated cylinder with a wall thickness of 1.1 mm, surrounded by tapered struts with a minimal diameter of 0.3 mm, was designed. In Figure 12 the polymeric template, additively manufactured with the Lithoz device, is depicted.

Preprints (www.preprints.org) | NOT PEER-REVIEWED | Posted: 4 February 2019 doi:10.20944/preprints201902.0027.v1

Peer-reviewed version available at Materials 2019, 12, 663; doi:10.3390/ma12040663

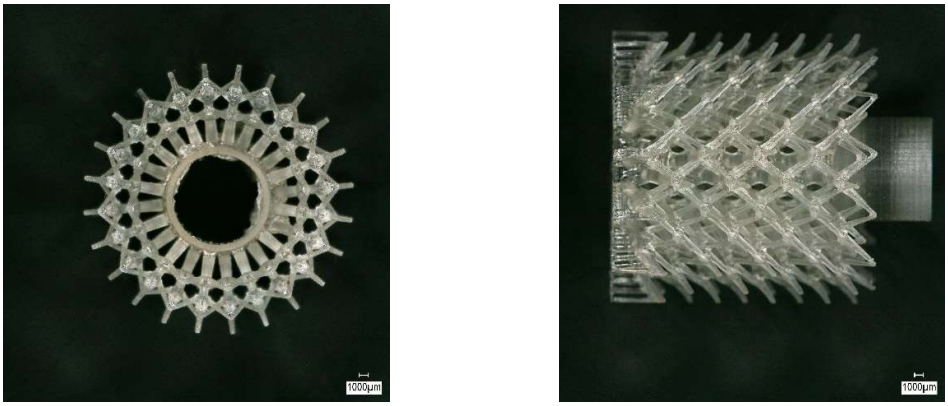

Figure 12: Complex structured polymeric template; left: top view; right: side view of generated polymeric template by stereo lithography

4.2.2. CerAM Replica – green and sintered components

The exact adjustment of the suspension´s rheology is mandatory to create an even coating on the template. In case of the SiC suspension, a homogeneous coating of all struts was found while all the defined pores between the strut network remained perfectly open. During the pyrolysis, the melting and outgassing template material induced small cracks at the base area, especially in the center ring holding the highest amount of template material. In contrast to this, all the other struts have survived the pyrolysis without any defects (Figure 13, left). Despite the shrinkage, no new cracks were observed in the structure after the completed sintering (Figure 13, right).

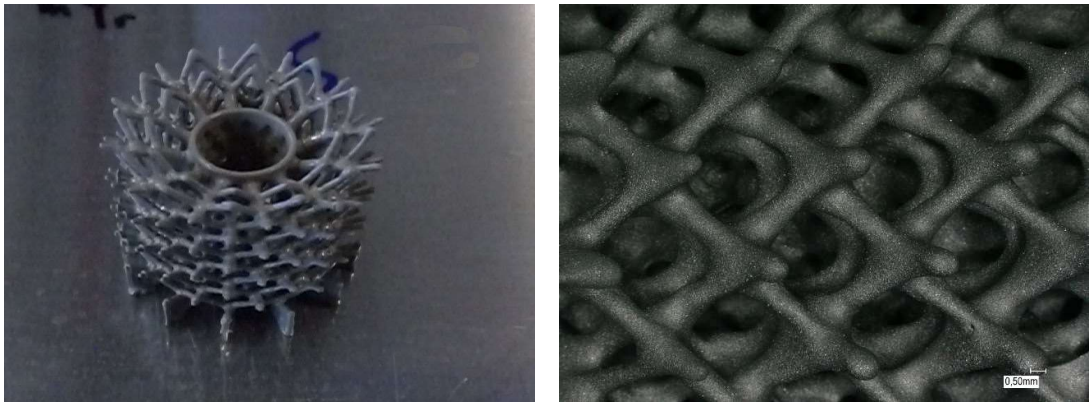

Figure 13: Replication of the polymeric template. Left: polymeric template with dry ceramic coating prior the heat treatment; Right: sintered SSiC struts.

4.2.3. CerAM Replica – characterization

The CT-analysis of the sintered component offers an interesting insight into the cavities created by the decomposed template and indicates the homogeneous coating of all struts (Figure 10).

Peer-reviewed version available at Materials 2019, 12, 663; doi:10.3390/ma12040663

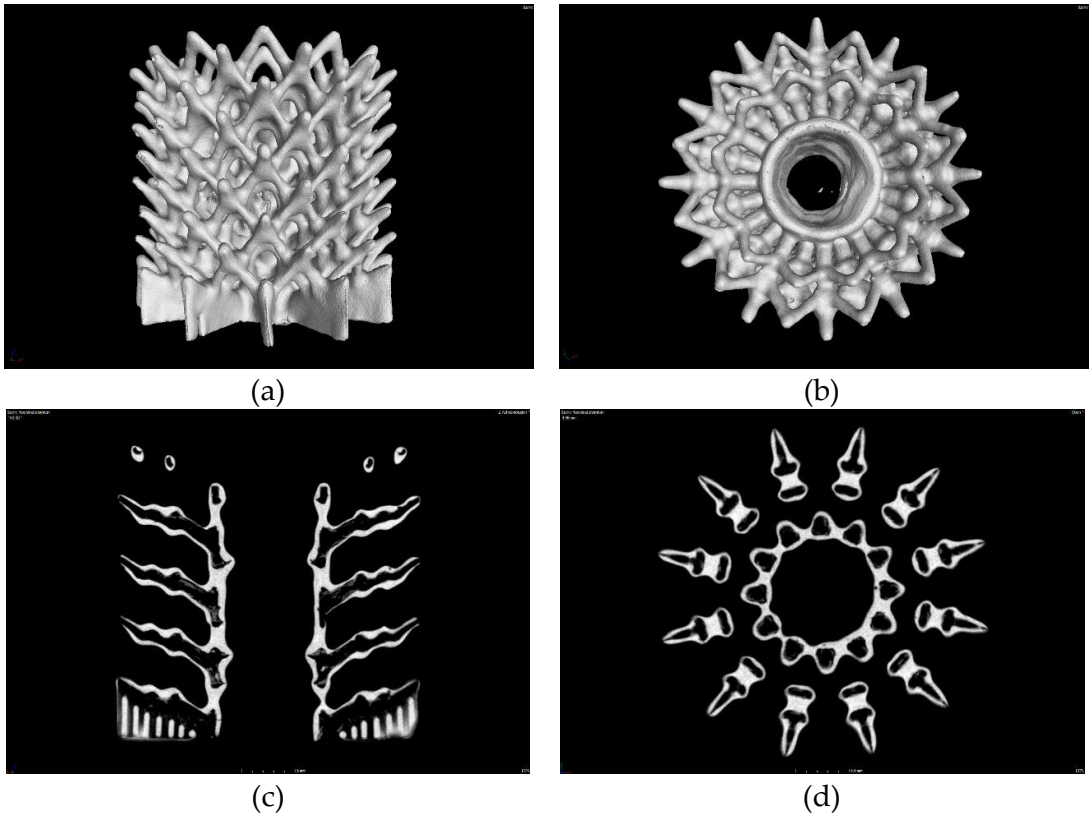

Figure 14: CT-analysis of the sintered SSiC structure: (a) side view, (b) top view, (c) vertical cut, (d) horizontal cut.

It is clearly visible that buried channels of various diameter and connectivity have been realized. The sintered SSiC leads to a mostly dense wall, separating the cavities from the surrounding open space in the structure. The accurate tapered tips at the end of the struts could be prepared as small jet nozzles, e.g. for burner structures.

4.3. CerAM T3DP

4.3.1. CerAM T3DP – characterization of the suspensions

Table 3 summarizes the calculated open porosity as results of the density measurements on the sintered test samples. For all three suspensions (A, D, H) the remaining open porosity after sintering at 1600 °C was below 0.5 %. But also the remaining open porosity of the samples manufactured with the suspensions with PFA were very low after sintering at 1600 °C.

The maximum content on PFA in the suspensions was limited to 10 vol.-%, because suspensions with higher amounts of PFA could not be processed reproducibly. But this porosity is too low for the addressed application. That is why the residual open porosities after sintering at 1250 °C were investigated. Due to the different sinter activity of the used powders the differences in the residual open porosity was much higher than after the sintering at 1600 °C. For the suspension D, which based on SMA6, a denser microstructure resulted, because of the higher sinter activity of the fine powder, whereas the powders CT1200 SG and MR52 were sintered partially, only.

Preprints (www.preprints.org) | NOT PEER-REVIEWED | Posted: 4 February 2019 doi:10.20944/preprints201902.0027.v1

Peer-reviewed version available at Materials 2019, 12, 663; doi:10.3390/ma12040663

Table 3: Calculated open porosity as result of the density measurements.

suspension	CT1200 SG	SMA6	MR52	PFA (10 Vol.-%)	open porosity [%] (after sintering at 1250°C)	open porosity [%] (after sintering at 1600°C)
A	x				28.85	0.46
B	x			x	30.22	4.45
C	x			x	24.05	
D		x			20.64	0.18
E		x		x	24.44	2.93
F		x			16.83	
G		x			8.49	
H			x		23.03	0.09
I			x	x	25.25	0.51

To increase the difference in the residual open porosities for the two suspensions B (CT1200 SG + PFA, open porosity: 30.22) and D (SMA6, open porosity: 20.64 %) the solid content of the suspensions were adjusted, more precisely. The solid content of suspension D was further increased as long as the printability was given to increase the density, whereas the solid content of suspension B was decreased as long as sedimentation occurs. A big challenge was the different shrinkage behavior of the suspensions. To process two suspensions together, a nearly equal shrinkage is necessary to avoid cracks. These developments resulted in the suspensions C and G, which was the best combination to produce nearly defect-free sintered multi-property components according to the CAD-model in chapter 3.3.1.

4.3.2. CerAM T3DP – green and sintered components

Different combinations of suspensions with and without PFA were used to manufacture multi-property components by CerAM T3DP. Figure 15 shows some green components, manufactured additively with two different suspensions. However, nearly all manufactured components contained small cracks after sintering at 1250 °C (Figure 16). Only some of the components based the suspension C and G could be sintered defect-free (Figure 16, right).

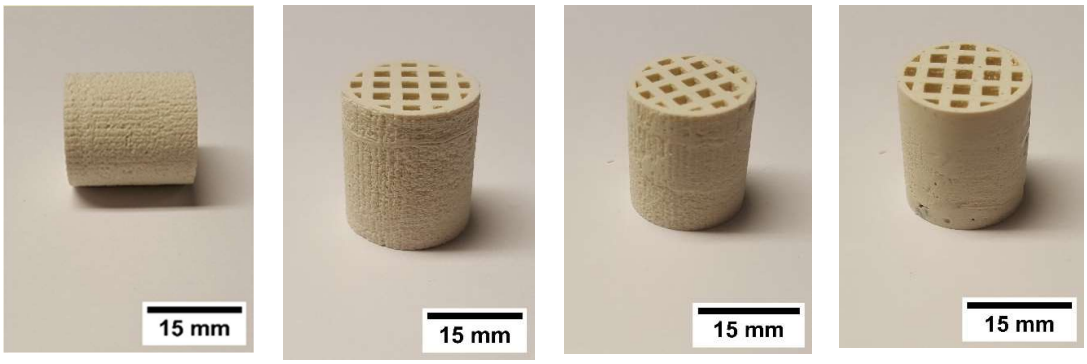

Figure 15: Honeycombs additively manufactured with different suspensions (left to right: C&G, C&G, C&G, A&F)

Preprints (www.preprints.org) | NOT PEER-REVIEWED | Posted: 4 February 2019 doi:10.20944/preprints201902.0027.v1

Peer-reviewed version available at Materials 2019, 12, 663; doi:10.3390/ma12040663

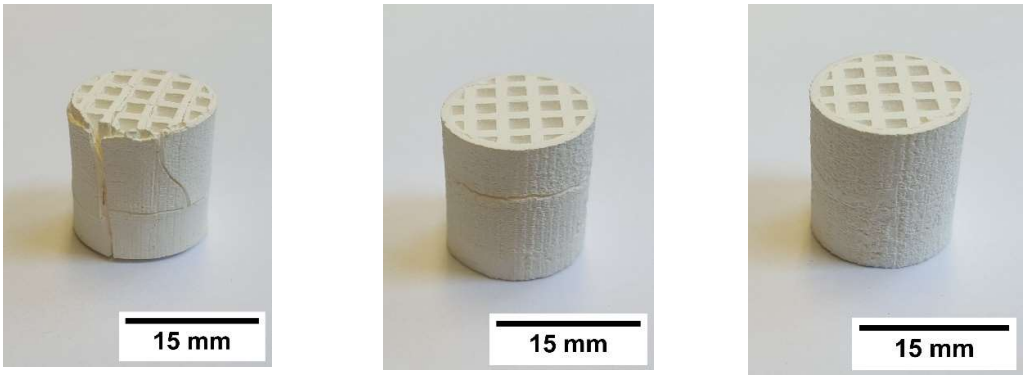

Figure 16: Sintered honeycombs manufactured with different suspensions (left to right: A&F, C&G, C&G)

To avoid cracking, the CAD-model was adapted and an additional cylindrical tube was added at the outside of the honeycomb. This structure was manufactured with the suspension C. This porous area had indeed no technological advantage but the shrinkage of the suspension G, which is higher than for suspension C, was limited. This increased the component quality after the sintering process further.

4.3.3. CerAM T3DP – characterization

To characterize the sintered CerAM T3DP components, SEM images of cross sections were taken. In Figure 17 the microstructure at the interface between the dense and the porous region is shown in different magnifications. A very good connection between the two regions is visible as well as the different microstructures, resulting from the different powders, which were used, and the added PFA.

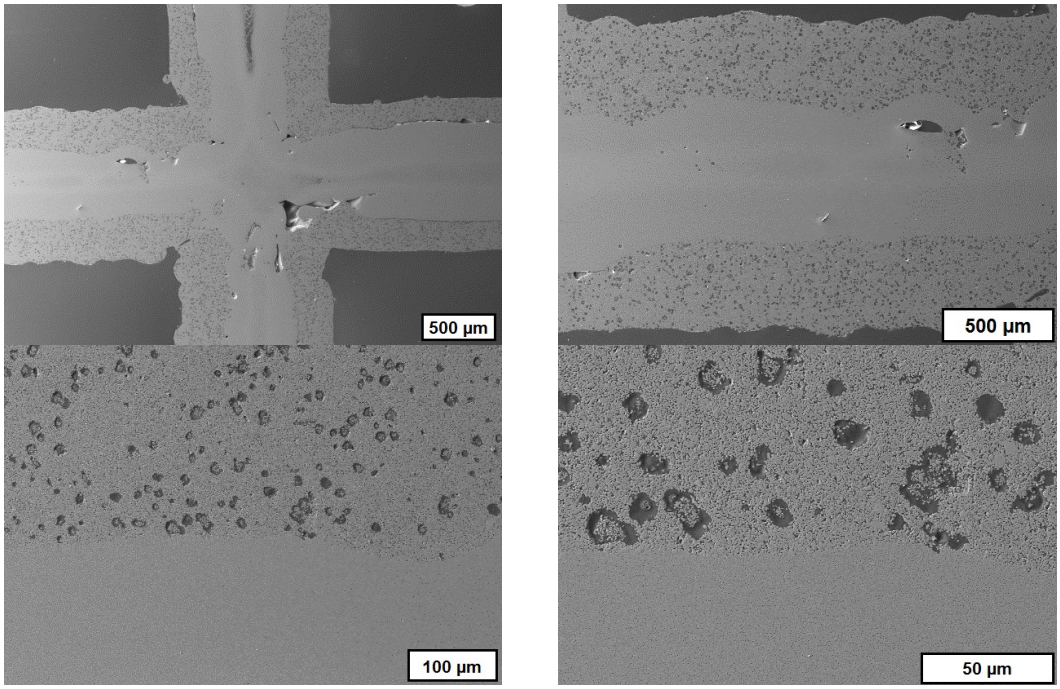

Peer-reviewed version available at Materials 2019, 12, 663; doi:10.3390/ma12040663

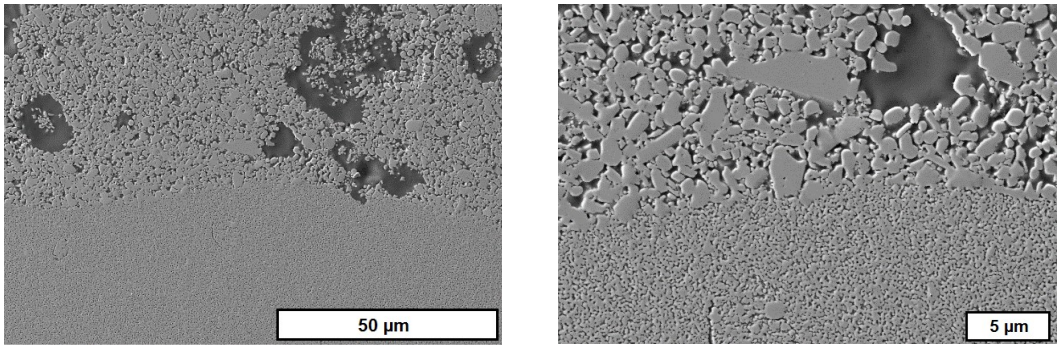

Figure 17: SEM images in different magnifications of cross sections of sintered ceramic dense-porous components additively manufactured by CerAM T3DP.

5. Conclusion

Different strategies for manufacturing of porous ceramic components were demonstrated. All of these strategies base on AM technologies and create new opportunities concerning the design and composition of the porous components, but there are specific restrictions, too.

Because of the high resolution and the very good properties of the sintered ceramic components, CerAM VPP is a very interesting approach to manufacture ceramic components with a macroscopic porosity additively. Furthermore, it would be possible to increase the porosity within the ceramic structures by the addition of PFA or the targeted variation of the sintering temperature. One of the main challenges is the generation of the needed CAD-data. Two different approaches were presented, which allow the manufacturing of ceramic components with geometries, which were not realizable so far. According to high accuracy, a further challenge is the cleaning of small pores deep within a structure. But in case of success, the CerAM VPP technology will be one of the most interesting AM methods to realize designed lattice pore structure of high-resolution.

CerAM Replica is a promising approach to generate innovative, porous ceramics. Based on a well-known process, this method enlarges the range of applications of porous ceramics due to its structural and functional flexibility. Especially the exploitation of the process-related cavities for the transport of media and/or reactants is remarkable. In addition, this method helps to overcome the lack of additive producible ceramics such as pressure-less sintered silicon carbide.

As a direct working AM technology CerAM T3DP is suitable for AM of multi-material and multi-property components, like dense-porous alumina components, which could be demonstrated in this work. Further investigations are needed to identify optimal suspension compositions and process parameters to manufacture nearly defect-free sintered, dense-porous ceramic components additively and to increase the porosity of the porous region.

Author Contributions: conceptualization, Uwe Scheithauer; methodology, validation, formal analysis, investigation and data curation: Florian Kerber, Steven Weingarten (CerAM T3DP), Alexander Füssel (CerAM Replica), Stefan Holtzhausen, Wieland Beckert (Designing, CAD-Data), Eric Schwarzer and Uwe Scheithauer (CerAM VPP); writing—original draft preparation and visualization, Florian Kerber, Alexander Füssel, Stefan Holtzhausen, Wieland Beckert, Eric Schwarzer, Steven Weingarten and Uwe Scheithauer; writing—review and editing, Uwe Scheithauer; supervision, project administration and funding acquisition, Uwe Scheithauer, Stefan Holtzhausen and Alexander Michaelis

Funding: Parts of this research was funded by German Federal Ministry of Education and Research, grant numbers 03ZZ0208A and 03ZZ0208I "Zwanzig20 - Agent-3D - Verbundvorhaben: FunGeoS".

Acknowledgments: The authors want to thank Mrs. Börner for their help during the finalization of the manuscript.

Conflicts of Interest: The authors declare no conflict of interest.

References

1. Adler, J.; Klose, T.; Piwonski, M. SiC-Keramik mit Porengrößen von nm bis µm. *Werkstoffwoche* **1998**, 3, 287-292.
2. Colombo, P. Conventional and novel processing methods for cellular ceramics. *Phil. Trans. R. Soc. A* **2006**, 364, 109–124.
3. Adler, J.; Standke, G. Open-celled foam ceramics, Part 1 and 2. *Keram.Z.* **2003**, 55 (9) 694-703; 55 (10), 786-792.
4. Luthard, F.; Adler, J.; Michaelis, A. Characteristics of a Continuous Direct Foaming Technique. International journal of applied ceramic technology 2015, 12 (S3), 133-138.
5. Schwartzwalder, A.V. et al. Method of making porous ceramic articles. US3090094 A, US-patent, 21. May **1963**.
6. Gauckler, L. J.; Waeber, M.M.; Conti, C.; Jacob-Duliere, M. Ceramic Foam for Molten Metal Filtration. *Journal of the Metals* **1985**, 37 [9], 47-50.
7. Fuessel, A.; Boettge, D.; Adler, J.; Marschallek, F.; Michaelis, A. Cellular Ceramics in Combustion Environments. *Advanced Engineering Materials* **2011**, 11, 13.
8. Zaversky, F. et al. Numerical and experimental evaluation of ceramic foam solar absorber - single-layer vs multi-layer configuration. *Applied Energy* 15. January **2018**, 351-375.
9. Boettge, D. et al. Functionalization of open-celled foams by homogeneous slurry based coatings. *Journal of Materials Research* 17. September **2013**, 28, 2220-2233.
10. Scheithauer, U.; Weingarten, S.; Abel, J.; Schwarzer, E.; Beckert, B.; Richter, H.-J.; Moritz, T.; Michaelis, A. Additive Manufacturing of Ceramic - Based Functionally Graded Materials Ceramic application, Munich, Germany 10.-13. April **2018**, 6 [2].
11. Homa, J. Rapid Prototyping of high-performance ceramics opens new opportunities for the CIM industry. Powder Injection Moulding International **2012**, 6 (3), 65-68.
12. Scheithauer, U.; Schwarzer, E.; Ganzer, G.; Körnig, A.; Beckert, W.; Reichelt, E.; Jahn, M.; Härtel, A.; Richter, H.-J.; Moritz, T.; Michaelis, A. Micro-reactors made by Lithography-based Ceramic Manufacturing (LCM). Proceedings of 11th CMCEE 2015, Vancouver, Ceramic Transactions **2016**, 258, ACERS, DOI: 10.1002/9781119236016
13. Scheithauer, U.; Schwarzer, E.; Moritz, T.; Michaelis, A. Additive Manufacturing of ceramic heat exchanger - Opportunities and limits of the Lithography-based Ceramic Manufacturing (LCM). JMEP **2018**, 27, 14-20, 10.1007/s11665-017-2843-z.
14. Frisken, S. F.; Perry, R. N. Designing with distance fields. ACM Press, **2006**. ACM SIGGRAPH 2006 Courses on - SIGGRAPH 06.
15. Bærentzen, J. A. und Aanæs, H. Generating Signed Distance Fields From Triangle Meshes. 2002. Tech. rep.
16. Lorensen, William E. und Cline, Harvey E. Marching cubes: A high resolution 3D surface construction algorithm. New York, NY, USA: ACM, 8 **1987**, SIGGRAPH Comput. Graph., Bd. 21, S. 163-169. ISSN: 0097-8930.
17. Zocca, A.; Colombo, P.; Gomes, C. M.; Günster, J. Additive Manufacturing of Ceramics: Issues, Potentialities, and Opportunities. Journal of the American Ceramic Society **2015**, 98 (7), 1983-2001, 10.1111/jace.13700.
18. Scheithauer, U.; Schwarzer, E.; Richter, H.J.; Moritz, T. Thermoplastic 3D Printing – An Additive Manufacturing Method for Producing Dense Ceramics. *Int. J. Appl. Ceram. Technol.* **2015**, 12 (1), 26-31, 10.1111/ijac.12306.
19. Scheithauer, U.; Johne, R.; Weingarten, S.; Schwarzer, E.; Abel, J.; Richter, H.; Moritz, T.; Michaelis, A. Investigation of Droplet Deposition for Suspensions Usable for Thermoplastic 3D Printing (T3DP). *Journal of Materials Engineering and Performance* **2018**, 27,1, 44-51, 10.1007/s11665-017-2875-4.
20. Scheithauer, U.; Pötschke, J.; Weingarten, S.; Schwarzer, E.; Vornberger, A.; Moritz, T.; Michaelis, A. Droplet-based additive manufacturing of hard metal components by thermoplastic 3D printing (T3DP). *Journal of Ceramic Science and Technology: An international Journal reporting on the synthesis, structure and properties of ceramics* **2017**, 8 (1), 155-160, 10.4416/JCST2016-00104.
21. Scheithauer, U.; Bergner, A.; Schwarzer, E.; Richter, H.-J.; Moritz, T. Studies on thermoplastic 3D printing of steel–zirconia composites. J Mat Res. 2014, 29 (17), 1931–1940, 10.1557/jmr.2014.209.

22. Scheithauer, U.; Slawik, T.; Schwarzer, E.; Richter, H.-J.; Moritz, T.; Michaelis, A. Additive Manufacturing of Metal-Ceramic-Composites by Thermoplastic 3D-Printing. J. Ceram. Sci. Tech. **2015**, 06 [02], 125-132.
23. Weingarten, S.; Scheithauer, U.; Johne, R.; Abel, J.; Schwarzer, E.; Moritz, T.; Michaelis, A. Multi-material Ceramic-Based Components – Additive Manufacturing of Black-and-white Zirconia Components by Thermoplastic 3D-Printing (CerAM - T3DP). J. Vis. Exp. **2019**, 143, e57538, 10.3791/57538.
24. Scheithauer, U.; Weingarten, S.; Johne, R.; Schwarzer, E.; Abel, J.; Richter, H.-J.; Moritz, T.; Michaelis, A. Ceramic-Based 4D Components: Additive Manufacturing (AM) of Ceramic-Based Functionally Graded Materials (FGM) by Thermoplastic 3D Printing (T3DP). Materials **2017**, 10, 19 pp. 10.3390/ma10121368.
25. Mitteramskogler, G.; Gmeiner, R.; Felzmann, R.; Gruber, S.; Hofstetter, C.; Stampfl, J. Light curing strategies for lithography-based additive manufacturing of customized ceramics. Additive Manufacturing **2014**, 1-4,110–118,10.1016/j.addma.2014.08.003c.
26. Johansson, E.; Lidström, O.; Johansson, J.; Lyckfeldt, O.; Adolfsson, E.; Influence of Resin Composition on the Defect Formation in Alumina Manufactured by Stereolithography. Materials **2017**, 10, 138, 10.3390/ma100020138.